Effects of Remaining Hair Cells on Cochlear Implant Function

15th Quarterly Progress Report

Neural Prosthesis Program
Contract N01-DC-2-1005
(Quarter spanning January-March, 2006)

K.V. Nourski, P.J. Abbas, C.A. Miller

Department of Otolaryngology-Head and Neck Surgery
&
Department of Speech Pathology and Audiology

University of Iowa

Iowa City, Iowa, USA

April 30, 2006

File: N01-DC-2-1005QPR15.PDF

Effects of Remaining Hair Cells on Cochlear Implant Function

N01-DC-2-1005QPR15

Neural Prosthesis Program

Table of Contents

1. Summary of Activities in This Quarter

During the fifteenth quarter of this contract (January 1 – March 31, 2006), we accomplished the following:

1. The manuscript entitled "Electrical excitation of the acoustically sensitive auditory nerve: Effects of acoustic stimulation" was accepted by JARO for publication. It details the feline animal model of the electrically stimulated and acoustically sensitive ear and provides comparisons between the electric responses of auditory nerve fibers (ANFs) of deaf and hearing ears.

2. We attended the Midwinter Meeting of the Association for Research in Otolaryngology (February 5 – 9, Baltimore, Maryland, USA) and made two presentations on the progress of our contract work (Miller *et al*., 2006; Nourski et al., 2006).

3. Charles Miller attended the Future of Cochlear Implants meeting (March 18-19, Ashland, MA; organized by Jim Patrick and Chris van den Honert) and presented a synopsis of the ANF work conducted under this contract relative to combined acoustic and electric stimulation.

4. We conducted a total of four acute-cat experiments. One experiments focused on single-fiber responses to electric pulse trains both masked and unmasked by a preceding electric pulse-train masker. That worked paralleled previous work conducted with ECAP measures (see QPRs 10 and 13). One experiments focused on obtaining additional electric-pulse train responses from ANFs from acutely deafened animals as a basis of comparison against responses from acoustically sensitive ANFs. The two remaining experiments involved obtaining both ANF responses and multi-unit responses from the inferior colliculus under conditions of electric and acoustic stimulation.

5. We completed the development of a MATLAB-based computational model of the auditory nerve fiber that allows for simulations of both electric and acoustic stimulation. Details and results of this work form the focus of this QPR.

6. We continued analysis of ANF response data from the aforementioned experiments.

7. We began writing a manuscript that will detail ANF responses to combined electric and acoustic stimulation.

2. Focus Topic: Model for combined electric and acoustic stimulation of the auditory nerve fiber

2.1. Introduction

Responses of the auditory nerve to continuous or repeated stimuli decrease over time, exhibiting the phenomenon of adaptation. Adaptation can result in greater sensitivity to changes that may occur during stimulation. Thus, it may aid the detection of novel stimuli and, consequently, contribute to speech perception.

Adaptation has been described for responses of the auditory nerve to acoustic stimuli (Eggermont & Spoor, 1973; Westerman & Smith, 1984; Javel, 1996) as well as electric stimuli (Javel, 1990; Killian *et al.,* 1994; Haenggeli *et al.,* 1998; Matsuoka *et al.,* 2000, Hu *et al.,* 2003). Adaptation in the auditory periphery follows a time course characterized by a rapid component (spanning a few milliseconds after stimulus onset), a short-term component (over a 50-100 ms epoch), a long-term long-term (over time intervals of seconds), and a very long-term (i.e., minutes) components (Westerman & Smith, 1984; Javel, 1996).

Adaptation and recovery from adaptation in the auditory periphery have been associated with several mechanisms (Eggermont, 1985; Chimento & Schreiner, 1991). These are release of neurotransmitter from inner hair cells, activation of neurotransmitter receptors at the postsynaptic membrane of peripheral processes of spiral ganglion neurons, and transmission of action potentials along the membrane of the auditory nerve fibers. Furukawa and Matsuura (1978) addressed adaptation of excitatory post-synaptic potentials in the eighth nerve afferents of the goldfish sacculus. They proposed presynaptic depletion of the neurotransmitter as a mechanism of adaptation. Application of these results to the mammalian peripheral auditory system was questioned by Chimento and Schreiner (1991), as the response properties of saccular afferent fibers are quite different from those in the mammalian auditory nerve fibers. More recently, Moser and Beutner (2000) described kinetics of neurotransmitter release in mouse inner hair cells. The depletion of the readily releasable pool of neurotransmitter was demonstrated to follow a time course similar to the adaptation of the auditory nerve responses. Most models of peripheral adaptation to acoustic stimulation are based on kinetics of neurotransmitter release at the inner hair cell-auditory neuron synapse (Schroeder & Hall, 1974; Smith & Brachman, 1982; Meddis, 1986; Sumner *et al*., 2002).

Chimento and Schreiner (1991) and Moser and Beutner (2000) suggested that although presynaptic neurotransmitter depletion might indeed contribute to auditory adaptation, it wasn't the only source of adaptation in the peripheral auditory system. Neurotransmitter receptors at the postsynaptic membrane of spiral ganglion neurons have also been suggested to play a role in the adaptation process. The proposed mechanism, based on the kinetics of receptor transition between free and occupied states, has been incorporated by Eggermont (1985) in his model of peripheral auditory adaptation.

Mechanisms that determine generation and transmission of action potentials in auditory nerve fibers are also relevant to adaptation of auditory nerve responses. The firing rate of auditory nerve fibers is limited by refractory characteristics of the neuronal membrane, described by the absolute and the relative refractory period (e.g., Miller et al., 2001). Membrane refractoriness has been implicated to play a role in adaptation, particularly in its rapid component (Eggermont, 1985). Refractory properties of nerve fibers may also produce summed effects that are not restricted to the rapid component of adaptation (Chimento & Schreiner, 1991). At any given time after the onset of a continuous or repeated stimulus, a fraction of auditory nerve fibers may be expected to be in a refractory state, producing a smaller population response.

In the case of electric stimulation of the deafened ear, contribution of synapse-related mechanisms to the phenomenon of adaptation is expected to be absent. Consequently, adaptation and recovery are likely to be limited to mechanisms associated with intrinsic properties of auditory nerve fibers (Killian *et al*., 1994). Computational models that describe responses of auditory nerve fibers to repeated electric stimuli limit time-dependent changes in neuronal excitability to a short-term refractory mechanism (Wilson *et al*., 1994; Bruce *et al*., 1999b), a significant shortcoming of previous efforts.

ECAP and single-fiber studies performed under this contract suggests that refractory and adaptation effects in the auditory nerve play an important role in interactions between responses to simultaneously presented electric and acoustic stimuli. One of the goals of our recent work has been to develop a computational model of the auditory nerve fiber's response to hybrid electric-acoustic stimulation. Such a model could be a useful tool for testing hypotheses regarding underlying mechanisms of acoustic-electric interactions in the auditory periphery. It could also allow one to predict auditory nerve fiber responses to novel stimuli (e.g., modulated pulse trains) and, hence, assist in the design and conduct of future experiments with real fibers. Of course, model validation studies are an essential first step.

This report summarizes our progress to date. We first outline the model design and its components. Model results and then presented, along with a preliminary evaluation of its validity by characterizing its output to electric and acoustic stimuli presented separately or simultaneously and comparing it to available physiological data.

2.2. Description of the model

The framework for this modeling approach was based upon elements of previous efforts, but with the novel addition of both acoustic and electric stimulus inputs and the incorporation of both refractory and adaptation processes. Thus, we began with model elements similar to that of Bruce *et al*. (1999a, 1999b) for electric stimulation and that of Schroeder and Hall (1974) for acoustic stimulation. Additional model stages and feedback were added to provide for interactions of refractoriness and adaptation introduced by either stimulus delivery mode. We note that the current version of the model assumes separate sites of auditory nerve fiber excitation for electric and acoustic stimuli. As such, it does not model the δ response. Also, electrical activation of the basilar membrane has not been incorporated; thus the β response is not represented.

Model components are summarized in Figure 1. The elements may be subdivided into three groups, associated with direct electric stimulation, acoustic stimulation and properties of the neuronal membrane, respectively. The model was implemented in MATLAB® Version 6.1 programming environment. Computer simulations were performed in a time-iterative manner with a sampling interval of 0.01 ms.

2.2.1. Direct electric stimulation

Simulation of auditory nerve fiber responses to electric stimuli was developed using the conceptual approach of the stochastic model proposed by Bruce et al. (1999a, 1999b). It is a threshold-crossing model, based on the comparison of the input stimulus potential with the threshold potential. When the stimulus potential [referred to as $v_e(t)$ in our model] is greater than the threshold potential [referred to as $v_{ethr}(t)$], an action potential is generated. Note that in our model the parameters and functions associated with electric stimuli are distinguished by subscript "*e*", those associated with acoustic stimuli are denoted by subscript "*a*" and those that correspond to properties of the neuronal membrane are marked with subscript "*m*".

Electric stimulus potential was calculated from electric stimulus current, $i_e(t)$, by taking into account the neuronal membrane's leaky-integrator property, implemented using the following impulse response function:

$$h(t) = e^{-t/\tau_m} \ , \tag{1}$$

where τ_m is the membrane time constant.

The electric stimulus current *vs.* time function, $i_e(t)$, was convoluted with the impulse response function to produce electric stimulus potential, $v_e(t)$:

$$v_e(t) = i_e(t) * h(t) \tag{2}$$

Threshold potential for the electric stimulus was calculated using the following formula:

$$v_{ethr}(t) = [V_{thr} + v_{enoise}(t)] \cdot \rho(t - t_{m0}) / n_m(t) \ , \tag{3}$$

where V_{thr} is the average threshold potential, $v_{enoise}(t)$ is the membrane noise potential, $\rho(t\text{-}t_{m0})$ is the refractory function and $n_m(t)$ is the membrane adaptation function.

Following the approach of Bruce et al. (1999a), the membrane noise potential, $v_{enoise}(t)$, was added to the average threshold potential, V_{thr}, to model random membrane threshold fluctuations (Verveen, 1961). It was determined as a random number drawn from a normal distribution with mean 0 and standard deviation σ_m. The value of v_e was compared with v_{ethr} to determine spike occurrence. If, within a given time interval, v_e was greater than or equal to v_{ethr}, a spike was said to occur in this time interval. The threshold potential and, consequently, spike generation in the modeled fiber, were affected by activity-dependent processes of refractoriness and adaptation (see Eq. 3). The refractory function, $\rho(t\text{-}t_{m0})$, was calculated as follows:

$$\rho(t - t_{m0}) = +\infty \ , \qquad \text{for } t - t_{m0} \le t_{abs} \tag{4a}$$

$$\rho(t - t_{m0}) = \frac{1}{1 - e^{-(t - t_{m0} - t_{abs})/\tau_{rel}}} \ , \text{ for } t - t_{m0} > t_{abs} \ , \tag{4b}$$

where t_{m0} is the time of the most recent spike, t_{abs} is the absolute refractory period, and τ_{rel} is the relative refractoriness time constant.

Activity-dependent membrane adaptation, $n_m(t)$, is a component of our model that was not present in the original model of Bruce et al. (1999a, 1999b). It was introduced to describe changes in the responsiveness of the auditory nerve fibers that occur on a longer time scale than refractory effects (*i.e.,* tens to hundreds of milliseconds). The initial value of n_m was set to 1. Immediately following each spike (*i.e.,* in the next time interval), the value of n_m decreased by a fixed percentage $p_m \cdot 100\%$:

$$n_m(t) = n_m(t - \Delta t) \cdot (1 - p_m) \tag{5a}$$

Then n_m recovered to 1 with a time constant equal to $1/r_m$:

$$dn_m / dt = r_m [1 - n_m(t)] \tag{5b}$$

2.2.2. Acoustic stimulation and spontaneous activity

To simulate the auditory nerve fiber's responses to acoustic stimulation as well as its spontaneous activity, we modified Schroeder & Hall's probabilistic model of hair cell-to-auditory neuron transduction (1974). Their original model is based on quantal generation and depletion of neurotransmitter in the hair cell. It is specified by three parameters:

1. r_a is the quantum (*i.e.,* synaptic vesicle) generation rate.

2. p_{a0} is the zero-signal probability of a quantum being released and causing an event (*i.e.,* "successful" release that can elicit an action potential).

3. g_a is the probability of a quantum being released and not causing an event (*i.e.,* loss of neurotransmitter without action potential generation).

In Schroeder & Hall's model, neurotransmitter quanta that evoke action potentials in the auditory nerve fiber are released with a probability of $f_a(t)$. It is proportional to a permeability function, $p_a(t)$ (related to the intensity of the input stimulus and rate of spontaneous neurotransmitter release) and number of available neurotransmitter quanta, $n_a(t)$.

The permeability function was calculated using a "soft" half-wave rectifier formula (Schroeder & Hall, 1974):

$$p_a(t) = p_{a0} \cdot \left[s_a(t)/2 + \sqrt{s_a^2(t)/4 + 1} \right], \tag{6}$$

where $s_a(t)$ is the acoustic stimulus waveform.

The number of available quanta in the hair cell was calculated from the model parameters using the following differential equation (Schroeder & Hall, 1974):

$$dn_a / dt = r_a - n_a(t) \cdot [p_a(t) + g_a] \tag{7}$$

This equation represents depletion of the neurotransmitter store and thus accounts for the synaptic component of peripheral auditory adaptation. It should be noted that it produces changes in the model output that are stimulus-dependent, rather than activity-dependent, as was the case for membrane adaptation $n_m(t)$ (see Eq. 5a,b).

Probability of vesicle release during a time interval Δt was defined by the formula:

$$f_a(t) = p_a(t) \cdot n_a(t) \cdot \Delta t \ , \tag{8}$$

Following calculation of $f_a(t)$, the occurrence of vesicle release was determined in a Monte-Carlo simulation, by comparing $f_a(t)$ with a random number.

In the original model of Schroeder & Hall (1974), each "successfully" released vesicle was essentially equivalent to a neural spike. In our model for combined electric-acoustic stimulation we employed a threshold-crossing approach, described above for direct electrically evoked neural excitation (see Eq. 2, 3). Thus, it was necessary to "convert" synaptic events (*i.e.,* vesicle release) into an input stimulus potential that could be compared with a threshold potential.

We resolved this by assuming that each released vesicle generated an excitatory postsynaptic current (EPSC), of amplitude I_a and duration t_a. The postsynaptic current *vs.* time function, $i_a(t)$, was then convoluted with the impulse response function (see Eq. 1) to produce the EPSP function, $v_a(t)$:

$$v_a(t) = i_a(t) * h(t) \tag{9}$$

We also assumed that excitation in response to neurotransmitter release by the hair cell occurred at a different site on the neuronal membrane than the excitation site in response to electric stimulation. We refer to these two distinct sites as site A (for "acoustic") and site E (for "electric") (see Figure 1). Consequently, threshold potential for hair cell-mediated excitation was calculated separately from the threshold for electric stimulation (*cf.* Eq. 3), using a different source of membrane noise:

$$v_{athr}(t) = [V_{thr} + v_{anoise}(t)] \cdot \rho(t - t_{m0}) / n_m(t) \ , \tag{10}$$

where $v_{anoise}(t)$ is the noise potential at the membrane site where hair cell-mediated excitation takes place, defined as a random number drawn from a normal distribution with mean 0 and standard deviation σ_m.

To determine spike occurrence in response to hair cell activity, the value of v_a was compared with v_{athr}, and the spike was generated in a given time interval if v_a was greater than or equal to v_{athr}.

2.2.3. Combined electric and acoustic stimulation

In the combined electric-acoustic model (see Figure 1), spikes may be evoked by either mode of stimulation. Threshold potentials for the two modes of excitation are affected by activity-dependent mechanisms of refractoriness, $\rho(t\text{-}t_{m0})$, and membrane adaptation, $n_m(t)$ in the same way (see Eq. 3, 10). Consequently, these two mechanisms provide a way in which acoustic stimuli (or spontaneous hair cell activity) may affect responses to electric stimuli, and *vice versa*.

2.2.4. Model parameters

The model parameters used in the simulations are summarized in Table 1. A sampling interval of 0.01 ms provided a reasonable resolution to describe the temporal properties of the model output (*i.e.*, spike latency and jitter).

The parameters that define the hair cell, p_{a0}=2.5, r_a=200 and g_a=7.5, were adjusted to provide a spontaneous firing rate of approximately 50 spike/s and a time constant of recovery of spontaneous firing rate following acoustic stimulation equal to 100 ms. Setting these three parameters to 0 provided a condition in which no neurotransmitter was generated or released in the modeled hair cell. Consequently, it allowed us to study the responses of the modeled auditory nerve fiber to electric stimuli in absence of hair cell-mediated activity (both spontaneous and acoustically driven).

The values of EPSC amplitude and duration (1 mA and 1 ms, respectively) were chosen to provide a one-to-one relationship between vesicle release from the hair cell and generation of an action potential in the auditory nerve fiber (provided that no refractory or adaptation effects occur).

For the time constant τ_m that describes the neuronal membrane integration properties, we used a value of 0.4 ms. Such a time constant corresponds to a chronaxie of 0.274 ms, which is the mean value reported by van den Honert & Stypulkowski (1984) for cat auditory nerve fibers stimulated with an intracochlear

electrode. Average membrane threshold, V_{thr}, and the standard deviation of membrane noise, σ_m, were set to 3 and 0.7 on an arbitrary voltage scale, respectively. These values were chosen to provide a realistic single fiber response threshold and relative spread of the growth function (see Results for the growth functions).

The parameters that describe the refractory properties of the modeled auditory nerve fiber are the absolute refractory period, t_{abs}, and the time constant of relative refractoriness, τ_{rel}. In our model, they were set to 0.7 ms and 1.3 ms, respectively [*cf*. the values of 0.7 ms and 1.32 ms used by Bruce et al. (1999b)].

Membrane adaptation is defined by the two parameters: decrement in excitability produced by each spike, p_m, and rate of recovery from adaptation, r_m. They were adjusted to the values of 0.02 and 10 s^{-1}, respectively, to provide a realistic time course of adaptation and recovery in the modeled single fiber responses (see Results for examples).

Table 1. Model parameters and their values		
Δt	Sampling interval	0.01 ms
p_{a0}	Zero-signal probability of a quantum being released and causing an event	2.5 s^{-1} *
r_a	Quanta generation rate	200 s^{-1} *
g_a	Probability of a quantum being released and not causing an event	7.5 s^{-1} *
I_a	EPSC amplitude	1 mA
t_a	EPSC duration	1 ms
τ_m	Membrane time constant	0.4 ms
σ_m	Standard deviation of membrane noise	0.7
V_{thr}	Average membrane threshold	3
t_{abs}	Absolute refractory period	0.7 ms
τ_{rel}	Relative refractoriness time constant	1.3 ms
p_m	Decrement in excitability produced by each spike	0.02
r_m	Rate of recovery from adaptation	10 s^{-1}

* To examine electrically evoked responses of the modeled fiber in a condition free of hair cell activity, these parameters were set to 0.

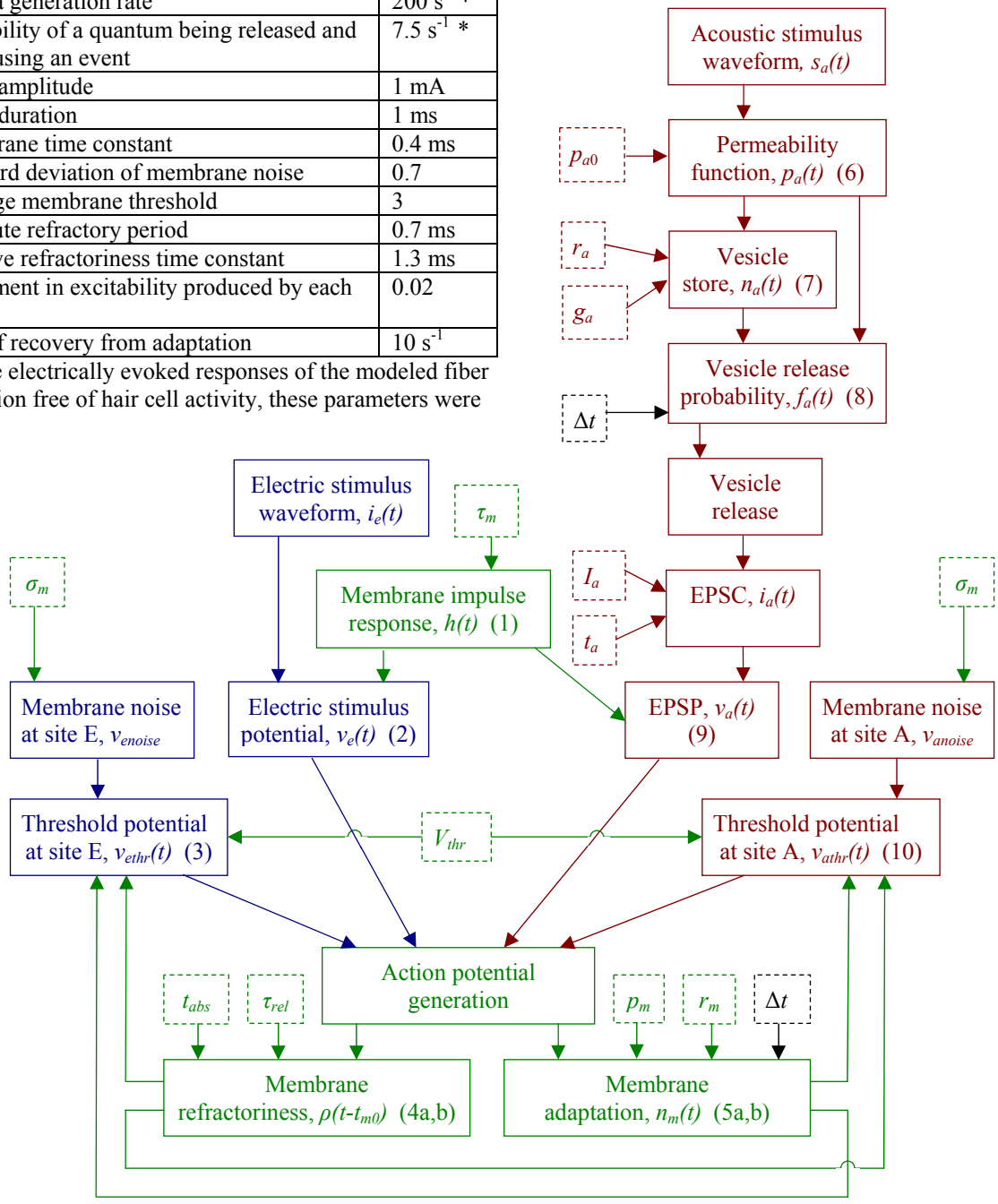

Figure 1. Schematic of the model. Model components associated with electric stimulation, acoustic stimulation and neuronal membrane properties are shown in blue, red and green, respectively. Model parameters are indicated by dashed boxes (see **Table 1** above for description); functions calculated by the model are indicated by solid boxes (numbers in parentheses indicate corresponding equations in text).

2.3. Results

In this section, we present a preliminary evaluation of the model by characterizing its output to electric stimuli, acoustic stimuli, and the two modes of stimulation combined. We also perform qualitative comparisons with physiological data; more quantitative comparisons will be presented in later reports.

For each stimulus, responses to 100 presentations (sweeps) were used to obtain peri-stimulatory time histograms (PSTHs), which were used to derive response properties of the modeled fiber (firing rate, latency, and jitter). Simulations were performed with a sampling interval of 0.01 ms. PSTHs shown in the present report were plotted using a 0.1 ms bin width, unless specified otherwise.

2.3.1. Responses to electric stimuli

First, we characterized the responses of the modeled auditory nerve fiber to electric stimuli (single pulses and pulse trains). The fiber was studied in two conditions: "silent" (without spontaneous hair-cell evoked activity) and with a spontaneous rate (SR) of approximately 50 spike/s. For the former condition, the parameters that define the hair cell (p_{a0}, r_a and g_a) were set to 0, and for the latter condition, they were set to 2.5, 200 and 7.5 s^{-1}, respectively (see Figure 1 and Table 1).

Figure 2 shows the model output to single, monophasic, electric pulses (duration 40 μs). In Figure 2A and 2B, examples of PSTHs obtained in response to a single 0.55 mA pulse are shown for the silent and spontaneously active fiber, respectively. To demonstrate the fine temporal structure of the responses, the PSTHs were plotted with a time bin equal to the sampling interval used in the simulation (*i.e.,* 0.01 ms).

Figure 2C illustrates changes in single-fiber firing efficiency (FE) across electric stimulus levels. FEs were obtained by first measuring the numbers of spikes within a 1 ms analysis window, then subtracting spontaneous activity, and normalizing responses to a percentage scale. The resultant growth functions had a realistic sigmoidal shape, consistent with physiological data on direct electrically evoked single-fiber responses (*e.g.*, Javel, 1990). In order to better illustrate the shape of the growth functions, the following equation was used to fit the simulation results:

$$FE(I) = \frac{a}{1 + e^{-(I - I_\theta)/b}} \tag{11}$$

Hair-cell mediated spontaneous activity appeared to affect the shape of the FE growth functions. Specifically, this condition yielded modest increases higher response threshold, θ, and relative spread of the growth function, RS (Verveen, 1961) (calculated as standard deviation of the growth function normalized to threshold).

Figures 2D and E provide a characterization of single-fiber temporal response properties. In these two panels, mean spike latency and jitter, respectively, are plotted as functions of FE. Results for a range of FEs between 10 and 90% are presented. Hair-cell activity did produce an effect on both latency and jitter of the electrically evoked single fiber responses. Both measures were generally greater in the spontaneously active fiber compared to the silent condition. Also, both mean spike latency and jitter decreased with stimulus level (trends are illustrated with linear regression lines in Figure 2D and 2E). These features of the model are consistent with physiological data (Miller *et al*., 1999; Miller *et al*., in press), although the physiological estimates of RS are somewhat lower than those produced by the model.

Figure 3 presents PSTHs of simulated single fiber responses to a 200 ms train of electric pulses presented at a rate of 250 pulses per second (pps). In both silent (panel A) and spontaneously active (panel B) conditions, clear adaptation to the electric stimulus was observed. In addition, peaks that correspond to highly synchronized electrically evoked responses were somewhat smaller in the modeled fiber that had spontaneous activity.

In Figure 4, the phenomenon of adaptation is demonstrated for several electric pulse rates. FE to each pulse of the train was measured over each interpulse interval (i.e., between the onset of adjacent pulses). FE exhibited greater decrements over time at higher pulse rates both in the silent and spontaneously active fiber. Also, at higher stimulation rates (500 pps and greater), the model output featured a clear refractory effect (a sharp decline in the FE to the second pulse). These trends are illustrated in Figure 5. Refractory FE was measured as FE to the second pulse normalized to the FE to the first pulse. Adapted FE was measured as the average FE to the pulses presented during the last 50 ms of the train normalized to the FE to the first pulse. Both the refractory and adaptation effects (as measured by the FE ratios) are greater at higher stimulus rates.

2.3.2. Responses to acoustic stimuli

To characterize the model output to acoustic stimuli, we generated responses to 200 ms bursts of acoustic noise (1 ms rise/fall time). Examples of model output generated using this approach are presented in Fig. 6 for five levels of acoustic noise. The model produced realistic PSTHs that featured spontaneous activity (evident during the 50 ms time interval prior to the noise onset), stimulus-dependent driven activity, adaptation (decrease in driven activity over time while the stimulus is on), as well as post-stimulatory depression and recovery of spontaneous firing. All these features are consistent with physiological data obtained from acoustically stimulated auditory nerve fibers (*e.g.*, Kiang *et al*., 1965; Westerman & Smith, 1984). Spontaneous firing rate was, on average, 49.4 spike/s.

Figure 7 presents rate-intensity functions for onset (A) and steady-state (B) acoustically evoked responses. Onset firing rates were calculated using a 1 ms analysis window at the onset of the acoustic stimulus. Steady-state firing rates were calculated using a 50 ms analysis window prior to the stimulus offset. Steady state firing rates were considerably smaller compared to onset rates, reflecting adaptation (note the Y-scale difference between panels A and B in Figure 7). To better illustrate the shape of the rate-intensity functions, we used a sigmoid function to fit the simulation results:

$$R(A) = \frac{a}{1 + e^{-(A - A_0)/b}} + 49.4 \text{ ,} \qquad (14)$$

The sigmoid appearance of these functions, the dynamic range of the steady-state response (around 30 dB) and saturation of steady-state driven activity at lower stimulus intensities compared to onset firing are consistent with physiological observations (Westerman & Smith, 1984).

2.3.3. Responses to combined electric and acoustic stimuli

Next, we examined whether the model could produce acoustic-electric interactions similar to those observed in our single-fiber data collected as part of this contract effort (see QPR #12). Figure 8 shows PSTHs obtained in response to 400 ms trains of electric pulses presented at a rate of 250 pps. Results obtained for four electric stimulus levels are shown.

In the responses shown in the left panels of Figure 8, electric pulse trains were presented alone. These PSTHs demonstrate a series of peaks that reflect the highly synchronized responses to the pulses of the train. In addition, background activity that corresponds to spontaneous firing was observed. In the right panels, a 200 ms burst of acoustic noise (level 80 dB SPL) was added at 50 ms after the onset of the pulse train. The PSTHs obtained in this condition featured a period of asynchronous activity that corresponded to the duration of the acoustic noise burst (indicated by a shaded horizontal bar). Following the offset of the noise, both background spontaneous activity and responses to electric pulses appeared somewhat decreased.

To examine changes in the modeled fiber's driven activity and firing synchrony more accurately, we performed interval analysis of the PSTHs using the same approach as in QPR #9 for physiological single fiber data. Measures of spike rates to individual pulses were obtained using 4 ms analysis windows (*i.e.*, the interpulse interval). Jitter was measured using 1 ms analysis windows (see Figure 2A). Next, the measures of spike rate and jitter were averaged across six wider time intervals of interest (Table 2; see also the bottom of Figure 8).

Table 2. Time windows used to analyze PSTHs.

Analysis interval	Interval duration (ms)	Interval description
1	20	Immediately after onset of the electric stimulus
2	30	Immediately before onset of the acoustic stimulus
3	20	Immediately after onset of the acoustic stimulus
4	30	Immediately before offset of the acoustic stimulus
5	30	5-35 ms after offset of the acoustic stimulus
6	100	Immediately before offset of the electric stimulus

Then the averaged spike rates and jitter values for each analysis interval in the "electric + noise" condition were normalized to the values obtained in the "electric only" condition. Figure 9 presents results of this analysis for a modeled fiber (left panels) along with analysis of data obtained from a cat auditory nerve fiber (right panels). In these plots, a value of 1 on the ordinate axis corresponds to no effect of the acoustic stimulus on responses to the electric stimuli presented within the given time interval. Acoustic noise produced an increase both in spike rate (Figure 9A) and jitter (Figure 9C) during intervals 3 and 4 (simultaneous effect of noise). Changes in both measures are smaller in interval 4 compared to interval 3. After the offset of acoustic noise there was a decrease in spike rate and jitter (post-stimulatory effect of noise). These changes are similar to those observed in physiological single-fiber data on combined electric-acoustic stimulation (*cf*. Figure 9 B, D; see also QPR #9, 12).

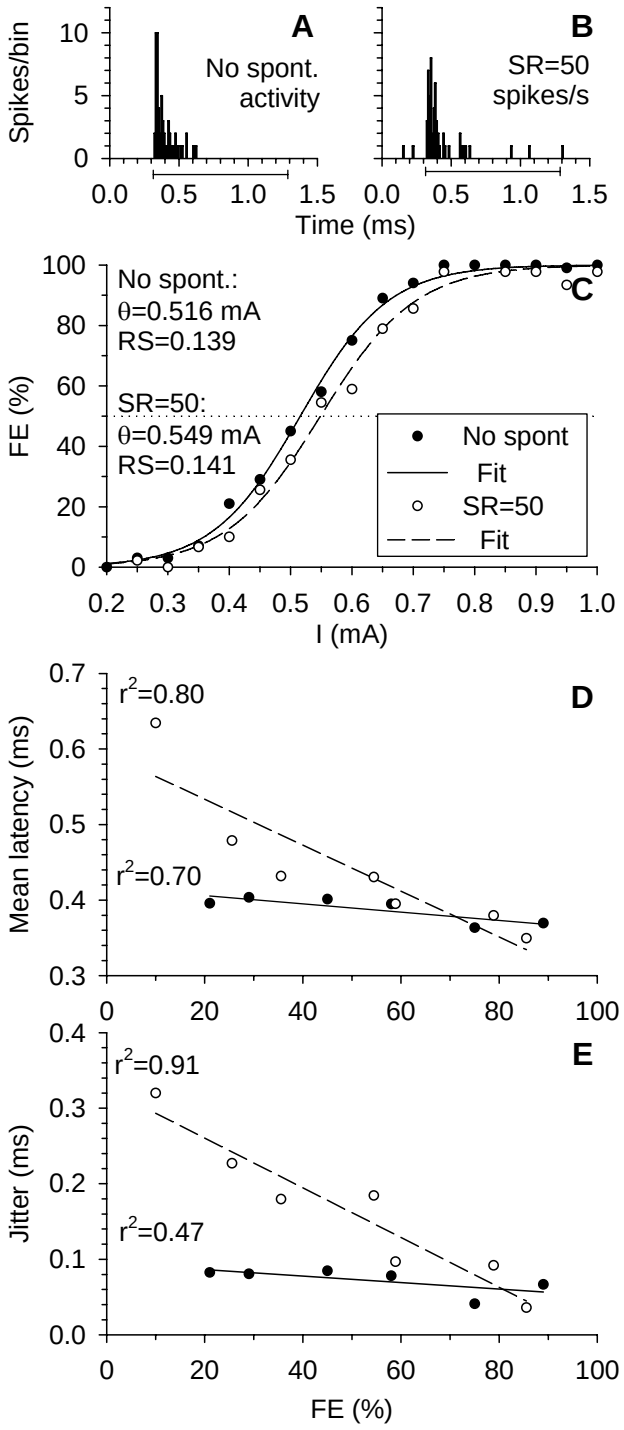

Figure 2. Model output to single monophasic electric pulses (duration 40 μs). **A**, **B**: Examples of PSTHs to a 0.55 mA pulse are shown for a fiber with no spontaneous activity and a spontaneous activity of approximately 50 spike/s, respectively. Bin width: 0.01 ms. Analysis windows (0.3-1.3 ms) are indicated below the graphs. **C**: Firing efficiencies are plotted as functions of electric stimulus level. Dotted line corresponds to fiber's response threshold (50% FE). **D**, **E**: Mean spike latencies and jitter, respectively, are plotted as functions of FE. In **C**, **D**, and **E**, results for a fiber that has no spontaneous activity and a spontaneous activity of approximately 50 spike/s are shown with filled and open symbols, respectively. Dotted line in (**C**) corresponds to fiber's response threshold (50% FE). SR, spontaneous rate. RS, relative spread.

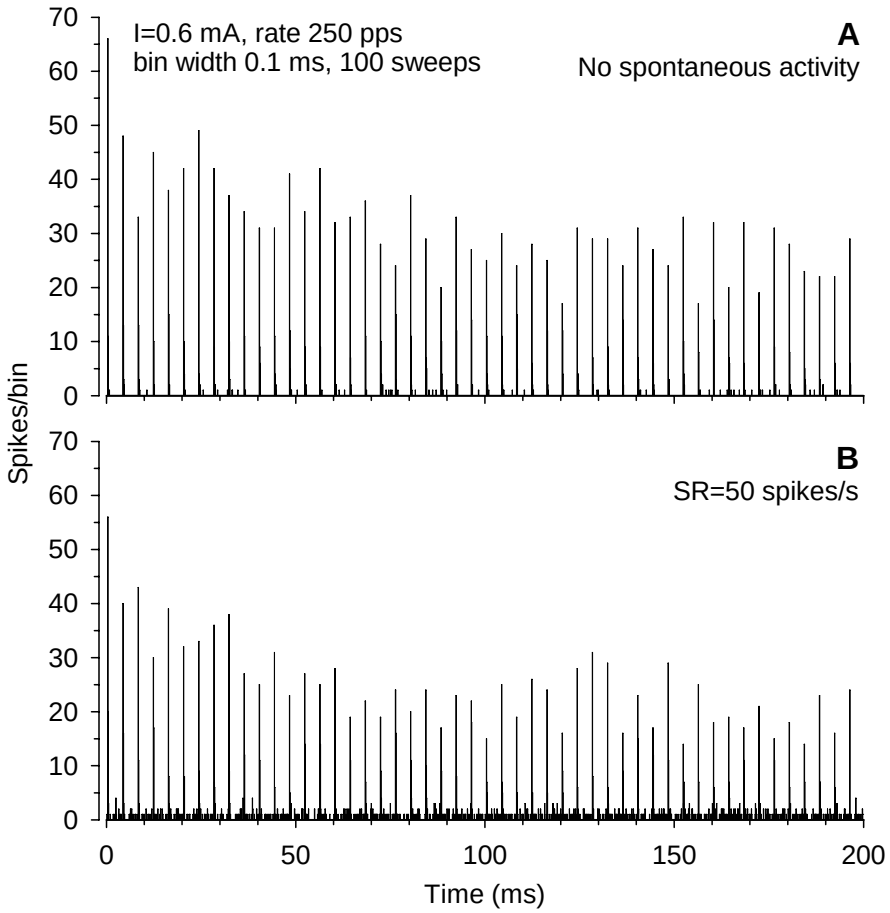

Figure 3. PSTHs of the model output to electric pulse train. Results for a fiber that has no spontaneous activity and a spontaneous activity of approximately 50 spike/s are shown in (**A**) and (**B**), respectively.

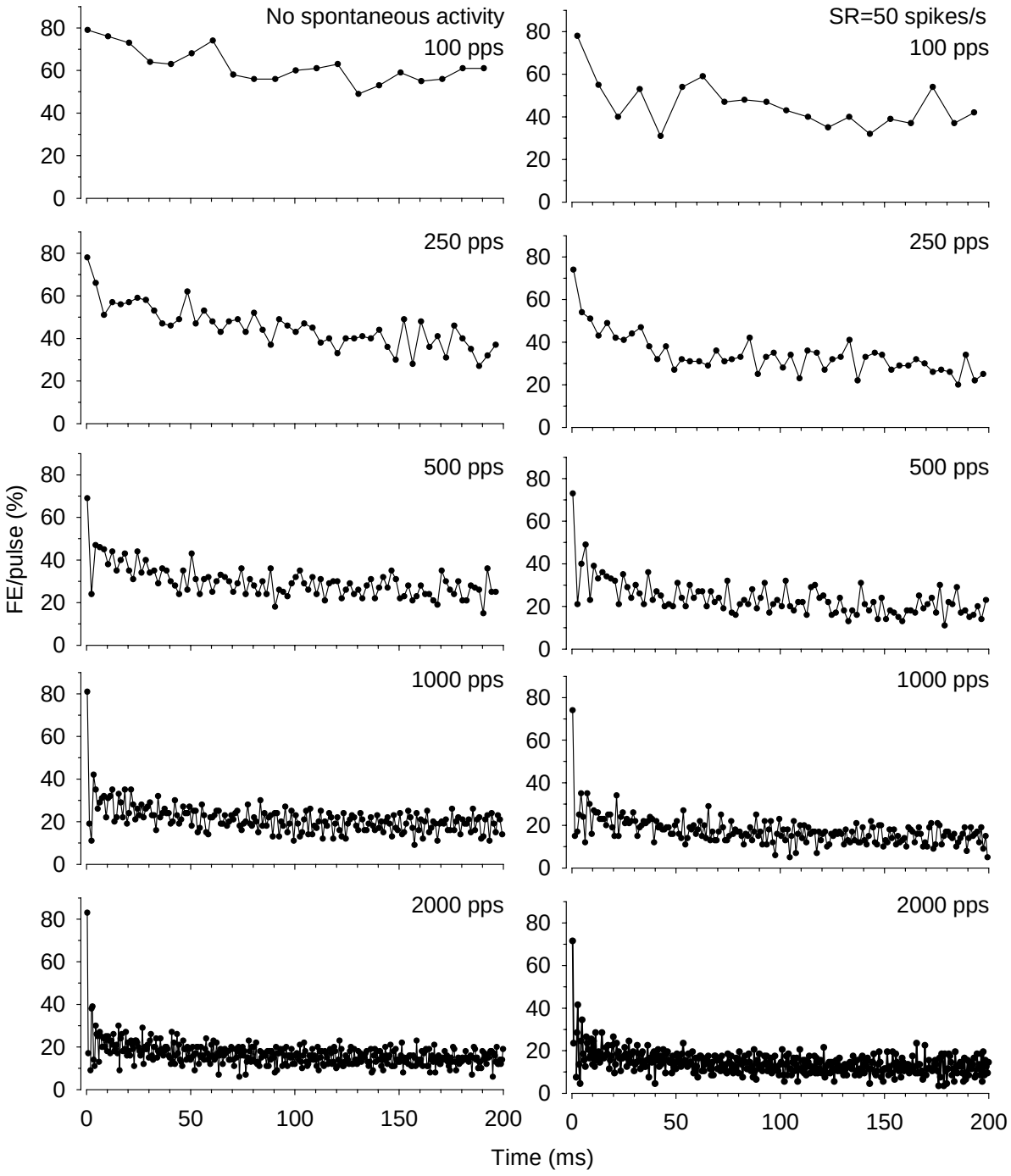

Figure 4. Model output to electric pulse train stimulation. Firing efficiency to pulses, calculated over intervals between the onset of the adjacent pulses, are plotted as functions of time. Results for a fiber that has no spontaneous activity and a spontaneous activity of approximately 50 spike/s are shown in left and right panels, respectively. Results obtained with five different pulse rates are presented.

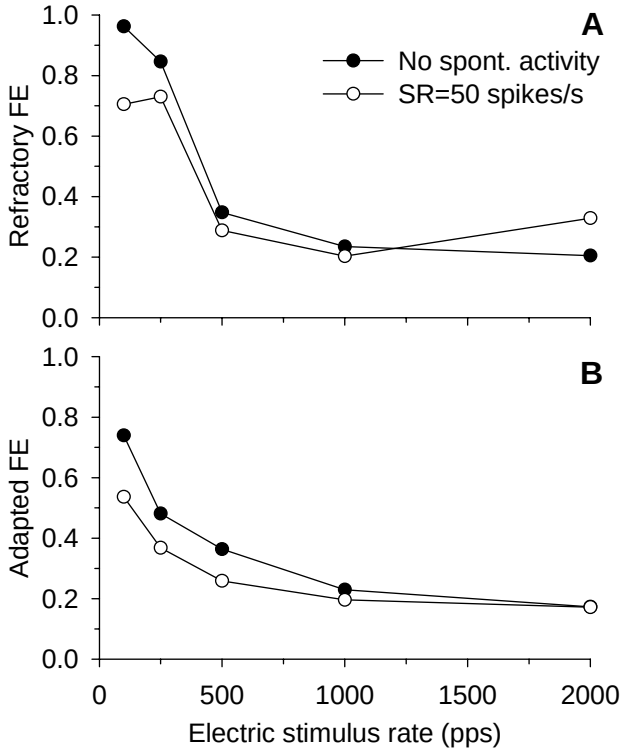

Figure 5. Refractoriness and adaptation in the modeled auditory nerve fiber responses to electric pulse trains. Refractory (**A**) and adapted (**B**) firing efficiencies are plotted as functions of electric stimulus rate for a fiber that has no spontaneous activity and a spontaneous activity of approximately 50 spike/s (filled and open circles, respectively). See text for details.

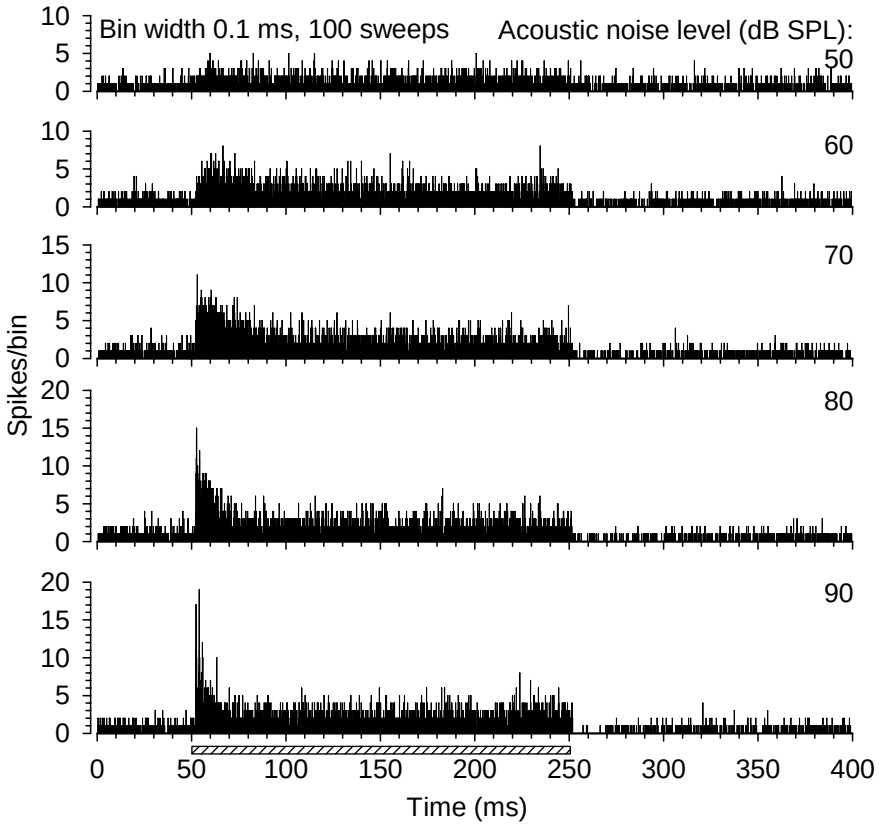

Figure 6. PSTHs of the model output to bursts of acoustic noise presented at different levels. Shaded horizontal bar indicates noise presentation time.

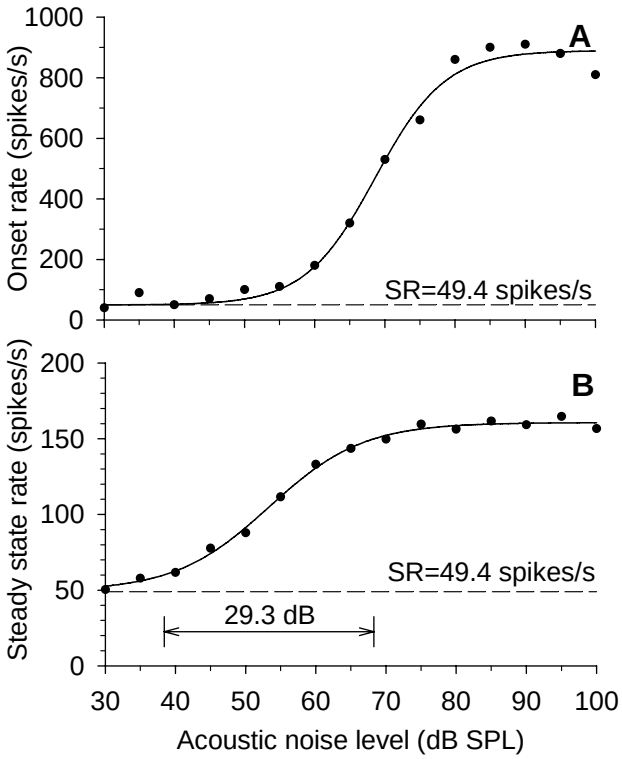

Figure 7. Model output to stimulation with 200 ms bursts of acoustic noise. **A**: Average firing rates at stimulus onset, calculated over a time window between 0.5 and 1.5 ms after stimulus onset, are plotted as a function of stimulus level. **B**: Average firing rates at steady state, calculated over a time window between 150 and 200 ms after stimulus onset, are plotted as a function of stimulus level. Dashed lines in (**A**) and (**B**) correspond to spontaneous firing rate, calculated over a time window of 50 ms prior to noise onset (see Figure 6). Stimulus range over which steady-state firing rate increases from 10% to 90% of the saturation rate is shown in (**B)**.

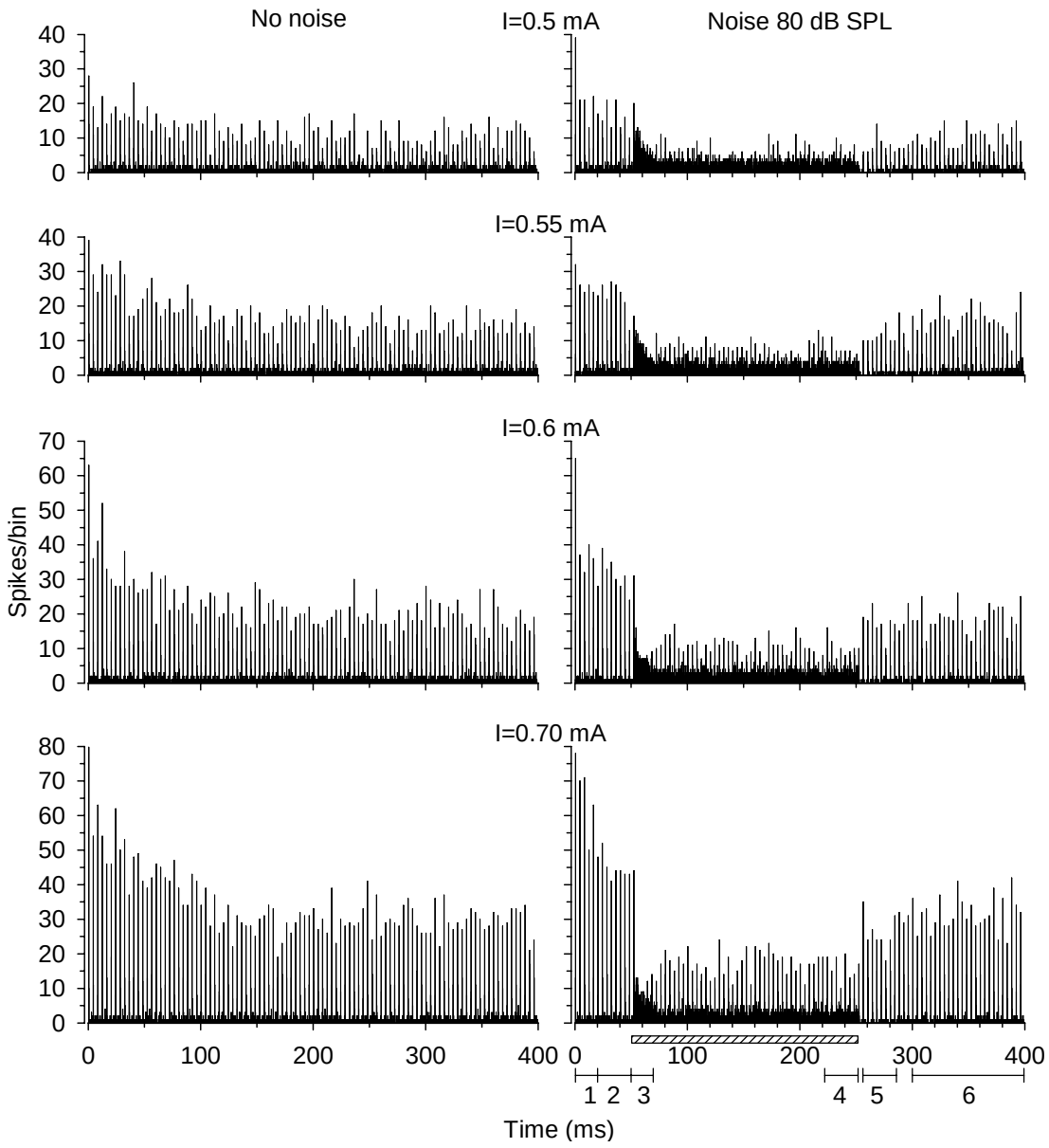

Figure 8. Model output to 400 ms 250 pps electric pulse trains presented without and with 80 dB acoustic noise (left and right panels, respectively). 0.1 ms bin width, 100 presentations. Shaded horizontal bar indicates noise presentation time. Intervals for subsequent analysis are shown on the bottom. See text for details.

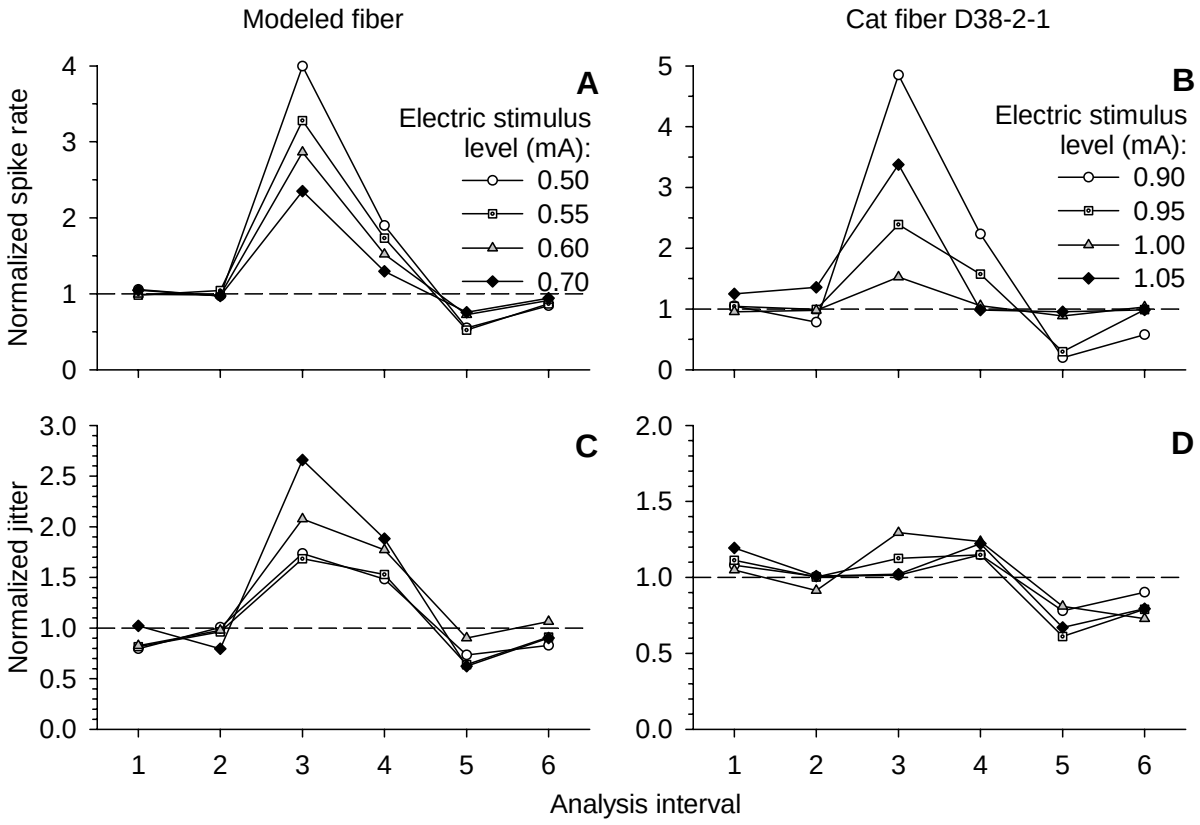

Figure 9. Effect of added acoustic noise stimulus on spike rate (**A, C**) and jitter (**B, D**) measures of single-fiber responses to electric pulse trains. Data obtained using our model and data from a cat auditory nerve fiber are shown in left and right panels, respectively. Results obtained with four electric stimulus levels are shown for both the modeled fiber and experimental data. Acoustic stimulus level was 80 dB SPL for the modeled fiber and 82 dB SPL for the fiber D38-2-1. See text for details.

2.4. Discussion

The computational model presented in this report demonstrates response properties that are at least qualitatively consistent with available physiological data. These properties include saturating input-output functions (see Figure 2C and 7), intensity dependence of spike latency and jitter (see Figure 2D and 2E), adaptation to both electric and acoustic stimuli (see Figure 3-7), and spontaneous activity (see Figure 6). In addition, the model provides simulations of key acoustic-electric interactions similar to those observed previously in our single-fiber data (see Figure 8, 9).

Also, although not presented here, we note that the membrane integration property, incorporated in the present model, can allow for generation of "build-up" responses, recently described in single-fiber responses to electric pulse trains (Miller *et al*., in press).

In this report, we demonstrated properties of the model using relatively simple stimuli (monophasic electric pulses and random acoustic noise). We note that arbitrary, more complex, stimuli (*e.g*., modulated pulse trains, speech-like envelopes) may be used with the model in its present form. In addition, the proposed single-fiber model may be used to develop a population model of the auditory nerve. Manipulation of model parameters and elements would be expected to provide information regarding the sensitivity of auditory nerve fiber response to specific manipulations. Some manipulations, such as altered time constants, would be expected to change with changes to a fiber's anatomical status, for example.

In its current form, the model has some significant limitations. However, in spite of those limitations, it is successful in demonstrating some key acoustic-electric interactions that involve refractory and adaptation effects. One weakness of the model is its intense computational requirements, which result in time-consuming estimates. Also, the current model does not account for spatial aspects of electric stimulation (e.g., differences between monopolar and bipolar stimulation due to different distribution of electric fields) or for a mechanism to simulate hair cell-mediated electrically evoked activity (electrophonic and δ-responses).

Membrane noise, v_{enoise} and v_{anoise}, modeled separately for the two sites of excitation (acoustic and electric) is not affected by either mode of stimulation or activity to either type of stimulus. As some physiological data and modeling results (Rubinstein *et al.*, 1999) suggest that membrane noise can increase during refractoriness, this phenomenon may be incorporated into the model, in the course of the model's further development.

The present model incorporates three time-dependent processes that affect excitability of the auditory nerve fiber. These are refractoriness, synaptic adaptation and membrane adaptation. The former two processes have physiological counterparts and are attributed to kinetics of voltage-gated Na^+ channels at the neuron and kinetics of neurotransmitter release at the hair cell, respectively. In contrast, specific molecular mechanisms underlying membrane adaptation remain unclear. It has been demonstrated that voltage-gated potassium channels containing Kv1.1 subunits could influence firing properties (maximum number of spikes and interspike intervals) of spiral ganglion neurons in response to depolarization (Adamson *et al*., 2002; Mo *et al*., 2002). Such channels localized in the neuronal membrane might therefore be contributing to adaptation in the auditory periphery (Mo *et al*., 2002). Other types of ion channels that might regulate firing patterns of auditory nerve fibers in response to continuous stimuli include large conductance Ca^{2+}-activated K^+ (BK) channels (Chen & Davis, 2006) and hyperpolarization-activated, cyclic nucleotide-gated (HCN) channels (Liu & Davis, 2006; Yi & Glowatzki, 2006).

In the present form of the model, we do not imply any specific molecular mechanism for membrane adaptation. We assumed an arbitrary function for this process, $n_m(t)$, (see Eq. 5a, 5b) that directly affected thresholds to acoustic and electric stimulation, v_{ethr} and v_{athr}, respectively (see Eq. 3, 10). An alternative approach is to model a stimulation- or activity-dependent process that would affect the input resistance of the neuronal membrane, and, consequently, change the membrane time constant, τ_m. This, in turn, would alter the membrane impulse response and, ultimately, membrane depolarization induced by electric and acoustic stimuli (v_{stim} and v_{epsp} , respectively; see Eq. 1, 2, 9). We plan to investigate this approach in the future.

3. Plans for the Next Quarter

In the next quarter, we plan to do the following:

1. Attend the 9th International Conference on Cochlear Implants (June 14-17, Vienna, Austria) and present results related to the contract work.

2. Attend the 5th Dutch Endo-Neuro-Psycho Meeting (June 4-9, 2006, Doorwerth, Netherlands) and present findings related to the research conducted under the present contract.

3. Continue collection and analysis of single-fiber data showing interaction of responses to combined electric and acoustic stimuli. Effects of electric stimuli on acoustically evoked responses and effects of pulse rate on responses to electric pulse trains will be particularly examined and incorporated with the model.

4. Extend the model results for quantitative comparison with physiological (single fiber and gross potential) auditory-nerve data.

5. Continue preparation of a manuscript detailing acoustic-electric interactions as observed by auditory nerve responses.

4. References

1. **Adamson, C.L., Reid, M.A., Mo, Z.L., Bowne-English, J., Davis, R.L. (2002).** Firing features and potassium channel content of murine spiral ganglion neurons vary with cochlear location. *J. Comp. Neurol.* 447:331-350.

2. **Bruce I.C., White, M.W., Irlicht, L.S., O'Leary, S.J., Dynes, S., Javel, E., Clark, G.M. (1999a).** A stochastic model of the electrically stimulated auditory nerve: Single-pulse response. *IEEE Trans. Biomed. Eng.* 46(6):617-629.

3. **Bruce I.C., Irlicht, L.S., White, M.W., O'Leary, S.J., Dynes, S., Javel, E., Clark, G.M. (1999b)**. A stochastic model of the electrically stimulated auditory nerve: Pulse-train response. *IEEE Trans. Biomed. Eng.* 46(6):630-637.

4. **Chen, W.C., Davis, R.L. (2006).** The role of Ca2+-activated K+ channel alpha and beta subunits in murine spiral ganglion neuron firing patterns. *Assoc. Res. Otolaryngol. 2006 MidWinter Meeting.* February 5 – 9, Baltimore, Maryland, USA. *Assoc. Res. Otolaryngol. Abs.:* 902.

5. **Chimento, T.C., Schreiner, C.E. (1991).** Adaptation and recovery from adaptation in single fiber responses of the cat auditory nerve. *J. Acoust. Soc. Am*. 90(1):263-273.

6. **Eggermont, J.J. (1985)**. Peripheral auditory adaptation and fatigue: A model oriented review. *Hear. Res*. 18:57-71.

7. **Eggermont, J.J., Spoor, A. (1973).** Cochlear adaptation in guinea pigs. *Audiology* 12:193-200

8. **Furukawa T, Matsuura S. (1978).** Adaptive rundown of excitatory post-synaptic potentials at synapses between hair cells and eight nerve fibres in the goldfish. *J. Physiol*. 276:193-209.

9. **Haenggeli, A., Zhang, J.S., Vischer, M.W., Pelizzone, M., Rouiller, E.M. (1998)**. Electrically evoked compound action potential (ECAP) of the cochlear nerve in response to pulsatile electrical stimulation of the cochlea in the rat: effects of stimulation at high rates. *Audiology* 37:353-371.

10. **Hu, N., Abbas, P.J., Miller, C.A., Robinson, B.K., Nourski, K.V., Jeng, F.C., Abkes, B.A., Nichols, J.M. (2003).** Auditory response to intracochlear electric stimuli following furosemide treatment. *Hear. Res*. 185:77-89.

11. **Javel, E. (1990)**. Acoustic and electrical encoding of temporal information. In: Miller J.M., Spelman F.A. (eds.). *Cochlear Implants: Models of the electrically stimulated ear*. Springer-Verlag, NY, pp. 247-295.

12. **Javel, E. (1996).** Long-term adaptation in cat auditory-nerve fiber responses. *J. Acoust. Soc. Am*. 99(2):1040-1052.

13. **Javel E., Tong Y.C., Shepherd R.K., Clark G.M. (1987).** Responses of cat auditory nerve fibers to biphasic electrical current pulses. *Ann. Otol. Rhinol. Laryngol*. 96(1II): 26-30.

14. **Kiang, N. Y.-S., Wanatabe, T., Thomas, E.C., Clark, L.F. (1965).** Discharge patterns of single fibers in the cat's auditory nerve. *Research Monograph No. 35*, MIT Press, Cambridge, MA.

15. **Killian, M.J.P., Klis, S.F.L., Smoorenburg, G.F. (1994).** Adaptation in the compound action potential response of the guinea pig VIIIth nerve to electric stimulation. *Hear. Res*. 81:66-82.

16. **Liu Q., Davis, R.L. (2006).** From apex to base: How endogenous membrane properties are distributed in the spiral ganglion. (2006). *Assoc. Res. Otolaryngol. 2006 MidWinter Meeting.* February 5 – 9, Baltimore, Maryland, USA. *Assoc. Res. Otolaryngol. Abs.:* 904.

17. **Matsuoka, A.J., Abbas, P.J., Rubinstein, J.T., Miller, C.A. (2000).** The neuronal response to electrical constant-amplitude pulse train stimulation: Evoked compound action potential recordings. *Hear. Res*. 149:115-128.

18. **Meddis, R. (1986).** Simulation of mechanical to neural transduction in the auditory receptor. *J. Acoust. Soc. Am.* 79(3): 702-711

19. **Miller, C.A., Abbas, P.J., Robinson, B.K., Rubinstein, J.T., Matsuoka, A.J. (1999).** Electrically evoked single fiber action potentials from cat: responses to monopolar, monophasic stimulation. *Hear. Res.* 119:142-154.

20. **Miller, C.A., Abbas, P.J., Robinson, B.K. (2001).** Response properties of the refractory auditory nerve fiber. JARO 2, 216-232.

21. **Miller, C.A., Abbas, P.J., Robinson, B.K., Nourski, K.V., Zhang, F., Jeng, F.-C. (in press).** Electrical excitation of the acoustically sensitive auditory nerve: Single-fiber responses to electric pulse trains. *J. Assoc. Res. Otolaryngol*.

22. **Miller C., Robinson B., Nourski K., Jeng F.-C., Abbas P. (2006).** Electrical stimulation of hearing ears: How the ECAP reflects single-fiber responses. *Assoc. Res. Otolaryngol. 2006 MidWinter Meeting.* February 5 – 9, Baltimore, Maryland, USA. *Assoc. Res. Otolaryngol. Abs.:* 1010.

23. **Mo, Z.L., Adamson, C.L., Davis, R.L. (2002).** Dendrotoxin-sensitive K+ currents contribute to accommodation in murine spiral ganglion neurons. *J. Physiol.* 542(3): 763-778.

24. **Moser, T., Beutner, D., (2000).** Kinetics of exocytosis and endocytosis at the cochlear inner hair cell afferent synapse of the mouse. *Proc. Natl. Acad. Sci. U.S.A*. 97(1): 883-888.

25. **Nourski K., Abbas P., Miller C., Robinson B., Jeng F.-C. (2006).** Forward masking of the electrically evoked compound action potential in animals with residual hair cell function. *Assoc. Res. Otolaryngol. 2006 MidWinter Meeting.* February 5 – 9, Baltimore, Maryland, USA. *Assoc. Res. Otolaryngol. Abs.:* 934.

26. **Rubinstein, J.T., Wilson, B.S., Finley, C.C., Abbas, P.J. (1999)** Pseudospontaneous activity: Stochastic independence of auditory nerve fibers with electrical stimulation. *Hear. Res*. 127, 108-118.

27. **Schroeder, M.R., Hall, J.L. (1974).** Model for mechanical to neural transduction in the auditory receptor. *J. Acoust. Soc. Am.,*55(5):1055-1060.

28. **Smith, R.L., Brachman, M.L. (1982)**. Adaptation in auditory-nerve fibers: A revised model. *Biol. Cybern.* 44:107-120.

29. **Sumner, C. J., Lopez-Poveda, E.A., O'Mard, L.P., Meddis, R. (2002).** A revised model of the inner-hair cell and auditory-nerve complex. *J. Acoust. Soc. Am.* 111(5): 2178-2188.

30. **van den Honert, C., Stypulkowski, P.H. (1984).** Physiological properties of the electrically stimulated auditory nerve. II. Single fiber recordings. *Hear. Res.* 14:225-243.

31. **Verveen, A.A. (1961).** Fluctuation in excitability. *PhD thesis*, University of Amsterdam, Amsterdam.

32. **Westerman, L.A., Smith, R.L. (1984)**. Rapid and short-term adaptation in auditory nerve responses. *Hear. Res*. 15:249-260.

33. **Wilson, B.S., Finley, C.C., Zerbi, M., Lawson, D.T. (1994).** Speech Processors for auditory prostheses, *7th Quarterly Progress Report*, Neural Prosthesis Program contract N01-DC-2-2401 NIH.

34. **Woo J., Abbas P., Noh H., Miller C., Nourski K., Robinson B., Hong S.H., Kim I.Y. (2006).** Acoustic-electric interactions in the inferior colliculus. *Assoc. Res. Otolaryngol. 2006 MidWinter Meeting.* February 5 – 9, Baltimore, Maryland, USA. *Assoc. Res. Otolaryngol. Abs.:* 100.

35. **Yi, E., Glowatzki, E. (2006).** Dendritic voltage-gated ion channels shape postsynaptic potentials at the inner hair cell afferent synapse. *Assoc. Res. Otolaryngol. 2006 MidWinter Meeting.* February 5 – 9, Baltimore, Maryland, USA. *Assoc. Res. Otolaryngol. Abs.:* 903.